ORIGINAL RESEARCH

Formability improvement with independent die and punch temperature control

Reza Bagheriasl · Kamyar Ghavam · Michael J. Worswick

Abstract A combined experimental and numerical study of the effects of die and punch temperature on the formability of a modified AA3003 aluminum alloy sheet for a case study sample is presented. Here, the non-isothermal deep drawing of a cup-like feature in a thin gauge aluminum automotive component is considered. An experimental forming setup that incorporates both heated dies and a cooled punch has been developed. A parametric study of the effects of die temperature, punch temperature, and blank holder force on the formability of the part is conducted. Numerical simulations of the warm forming process are performed using a coupled thermo-mechanical finite element model. The temperature-dependant material model combines the Bergstrom hardening rule with Barlat's YLD2000 yield function and was implemented in LS-DYNA as a user-defined material model. Selected experimental cases were modelled numerically and compared to experiments. The FEA model was validated against experimental results by comparing measured and predicted punch force versus displacement as well as trends in the formability as a function of die temperature.

Keywords Warm forming · Non-isothermal deep drawing · AA3003 aluminum alloy sheet · Strain-rate sensitive flow rule · Anisotropic yield surface

R. Bagheriasl (✉) · K. Ghavam · M. J. Worswick
Mechanical and Mechatronics Engineering Department,
University of Waterloo,
200 University Ave.,
West Waterloo, Ontario N2L 3G1, Canada
e-mail: rbagheri@uwaterloo.ca

Introduction

Recently, the aerospace and automotive industries have been using lightweight structures as a means to improve fuel efficiency and reduce emissions. Aluminum alloys are considered suitable replacements for mild steel structures because of their low density, comparable strength, and stiffness to reduce weight. However, the forming of aluminum alloy sheet with conventional forming technologies into desired complex shapes is often difficult and not cost-effective due to the requirement of using multiple forming steps since the formability of these alloys under room temperature conditions is limited. Warm forming has been considered widely to improve the formability of aluminum alloy sheet by performing the forming operation at an elevated temperature lower than the recrystallization temperature [30]. The most important advantage of warm forming is that the forming limit strains at elevated temperatures are increased significantly allowing complex geometries to be achieved by this method. The challenge for process design is the complexity and interaction of mechanical and thermal effects on the process.

Warm forming was studied by Shehata et al. [28] and Wilson [31] who demonstrated that warm forming improves the formability of AA5082 and AA5005 since the strain hardening of these alloys increases at elevated temperatures. Li and Ghosh [20] have shown that warm forming can considerably improve the formability of aluminum alloy sheet.

Partial heating in the holder or die area has been shown to produce a much better effect on formability than uniformly heated tools [26,27]. Naka and Yoshida [23] studied deep drawing of AA5083 with different die temperatures and a water cooled punch. Takuda et al. [29] studied the

deformation behaviour and the temperature change in non-isothermal deep drawing of AA5182-O aluminum alloy sheet and showed that the LDR in warm deep drawing increases with the temperature of the die profile radius. Boogaard and Huetink [10] and McKinley et al. [22] studied cylindrical cup deep drawing at different gradients of temperature and observed that the formability of Al–Mg sheet can be improved by increasing the temperature in some regions of the sheet and cooling other regions. Similar results were found by Palumbo and Tricarico [25] for AA5754-O forming and by Kaya et al. [16] for AA5754 and AA5052 alloys.

Finite element analysis is an important tool for part and tooling design. In order to accurately capture the behaviour of aluminum alloy sheet within numerical simulations, proper constitutive equations must be used. Aluminum alloys display anisotropic behaviour in the plastic region, requiring anisotropic yield criteria. In particular, this includes capturing material R-values which control thinning in textured sheet materials and reflects the crystallographic nature of the yield surface. The Barlat YLD2000 yield surface [6] has been shown to accurately describe the anisotropic material behavior of aluminum alloy sheet [2–5,14,15]. Another important consideration for modeling aluminum alloys is the hardening response and the complex interaction between strain rate sensitivity and thermal softening. Traditional hardening models describe the flow stress in terms of mathematical equations, such as power laws, with empirical constants fit to experimental data. Such empirical models are often limited in terms of their consideration of the metal physics governing the material behaviour. In spite of the fact that empirical models have been used extensively in FEM codes, they are often unable to predict material behaviour beyond the range of measured data. Physically motivated models, which model microstructure evolution indirectly, may have a wider applicability. Such models consider the evolution of dislocation density [9,24] to predict strength and assume storage and recovery to be the main mechanisms controlling dislocation density evolution.

Recently, warm forming simulation of anisotropic elastoplastic hardening materials has been studied, using temperature/strain rate dependent hardening rules. Farrokh and Khan [12] proposed a new formulation for flow stress in terms of temperature, strain rate and grain size for ultra-fine grained and nanocrystalline copper and aluminum. Ghavam and Naghdabadi [13] introduced a constitutive model with a temperature and strain rate dependant flow stress based on the Bergstrom hardening rule and modified Armstrong-Frederick kinematic evolution equation for elastoplastic hardening materials. The reported constitutive fitting exercises have identified the Bergstrom [10] or NES [18,19] models as appropriate hardening models for use in numerical simulation of warm forming.

While the aforementioned studies have reported the application of the NES/Bergstrom model and the Barlat-2000 yield surface separately; the current work considers the novel implementation of the Barlat YLD2000 yield surface in conjunction with the Bergstrom hardening model to accurately model aluminum alloy sheet during warm forming.

In this paper, experiments and simulations of the warm forming process for a simplified plate component that represents the fluid channel and manifold of an automotive heat exchanger were developed in order to assess the potential formability gain that could be achieved relative to conventional room temperature metal forming processes. The experiments were also used to assess the effectiveness of the numerical model to simulate the aluminum alloy warm forming processes. A partial section of a plate component with a cup feature incorporated at one end (Fig. 1) was considered for this study. The aluminum alloy used was a brazing sheet composite representative of the production component material, consisting of a modified AA3003 core alloy.

The plate tooling geometry was generated based on a plate design provided by Dana Canada which incorporates the deep drawn cup feature. In normal room temperature manufacturing of the plates, multiple forming steps are required to achieve the depth of draw needed to form the cup feature within the limited width of the plate geometry. One objective of this work is to determine whether warm forming, in particular non-isothermal warm forming with a cold punch and heated die, would allow a plate to be formed in a single draw step. The goal is to maximize the formability of the material and to form the part (i) without failure or necking and (ii) without excessive wrinkling in the flange region.

A constitutive model for elastoplastic hardening materials with induced anisotropy including the Bergstrom model and Barlat YLD2000 anisotropic yield function [15] was used and implemented as a user defined material subroutine (UMAT) in LS-DYNA. Numerical models of the non-isothermal forming of the part were performed. The results
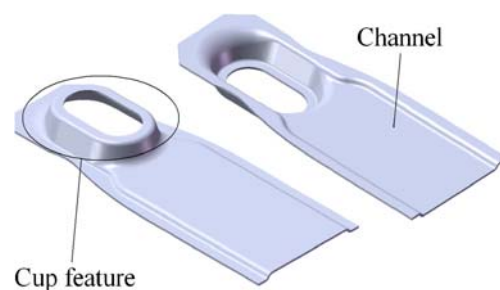

Fig. 1 Schematic view of a simplified plate component with a cup feature at one end. These plates are stacked and brazed together to form the manifold and fluid channel of an automotive component

of the numerical models have been validated against the corresponding experimental data.

Constitutive modeling and the governing equations

A user-defined material subroutine (UMAT) embodying the Bergstrom model to capture the dependence of work hardening on strain rate and temperature, in conjunction with the Barlat YLD2000 yield function to describe the anisotropic behaviour of FCC aluminum alloys at elevated temperatures has been developed. This section presents the primary equations required within the UMAT developed for this paper.

Flow stress and hardening

The flow stress of aluminum alloy sheet is well described by the physically-based Bergstrom model [9]. The model is able to take into account the evolution of the dislocation density due to work hardening and dynamic recovery. The flow stress, $\overline{\sigma}$, in the Bergstrom model is composed of a temperature dependent term, a dynamic stress term depending on the strain rate and temperature, and finally a work hardening term that depends on both dislocation density and temperature, as expressed by

$$\overline{\sigma} = \left(1 - C_T exp\left(-\frac{T_1}{T}\right)\right)\left(\sigma_0 + \alpha G_{ref} b\sqrt{\rho}\right) \quad (1)$$

The evolution of the dislocation density ρ is responsible for the hardening. Also, the dynamic recovery term is due to annihilation and remobilization of dislocations. In Eq. (1) C_T and T_1 are fitting parameters for the temperature dependency function, G_{ref} is the reference shear modulus, α is a scaling parameter of order unity [10], b is the Burgers vector, σ_0 is the initial yield stress and ρ is the dislocation density which evolves during the deformation from its initial value, as described by

$$\frac{d\rho}{d\varepsilon} = U_0\rho - \Omega\left(\dot{\varepsilon}, T\right)\rho \quad (2)$$

where U_0 is a fit parameter. The first term in the right hand side, describes the storage of mobile dislocations, and Ω describes the dynamic recovery due to remobilization and annihilation, which is defined as follows

$$\Omega = \Omega_0 + Cexp\left(-\frac{mQv}{RT}\right)\dot{\varepsilon}^{-m} \quad (3)$$

Where R is the gas constant, Q_v is the activation energy for vacancy migration and C and m are two fit parameters.

Yield criterion

The anisotropic yield function for plane stress in the x-y plane in general format is expressed by Barlat et al. [6] as:

$$\phi = \left|S_1' - S_2'\right|^a + \left|2S_2'' + S_1''\right|^a + \left|2S_1'' + S_2''\right|^a = 2\overline{\sigma}^a \quad (4)$$

where a=8 for FCC materials and $S_{1,2}'$ and $S_{1,2}''$ are the principal values of the linear transformations of the stress deviators tensors; S' and S'', which are defined as

$$S' = L'.\sigma$$
$$S'' = L''.\sigma \quad (5)$$

In Eq. (5) L' and L'' are the transformation matrices and are expressed as

$$\mathbf{L'} = \frac{1}{3}\begin{bmatrix} 2 & 0 & 0 \\ -1 & 0 & 0 \\ 0 & -1 & 0 \\ 0 & 2 & 0 \\ 0 & 0 & 3 \end{bmatrix}\begin{bmatrix} \alpha_1 \\ \alpha_2 \\ \alpha_7 \end{bmatrix}, \quad \mathbf{L''} = \frac{1}{9}\begin{bmatrix} -2 & 2 & 8 & -2 & 0 \\ 1 & -4 & -4 & 4 & 0 \\ 4 & -4 & -4 & 1 & 0 \\ -2 & 8 & 2 & -2 & 0 \\ 0 & 0 & 0 & 0 & 9 \end{bmatrix}\begin{bmatrix} \alpha_3 \\ \alpha_4 \\ \alpha_5 \\ \alpha_6 \\ \alpha_8 \end{bmatrix}$$

$$(6)$$

The independent coefficients α_i describe the anisotropic behaviour of a material. For the material model to account for changes in temperature, the anisotropy coefficients must be expressed in terms of temperature. They reduce to unity in the isotropic case, in which the YLD 2000 model returns to a von Mises yield criterion. Seven coefficients can be determined using the yield stresses in the longitudinal, transverse and diagonal directions and biaxial yield stress, namely σ_0, σ_{45}, σ_{90}, σ_b and R-values R_0, R_{45} and R_{90}. The eighth coefficient can be determined by assuming $L_{12}'' = L_{21}''$, or by using additional input data such as the ratio $R_b = \dot{\varepsilon}_{xx}/\dot{\varepsilon}_{yy}$, which characterizes the slope of the yield surface in balanced biaxial tension ($\sigma_{xx} = \sigma_{yy}$). Since biaxial data was unavailable, σ_b is set equal to ($\sigma_0 + \sigma_{45}$)/2 [1].

Table 1 Mechanical properties and Bergstrom fit parameters for aluminum alloy AA3003

μ_0=26354 MPa	m=0.4239	Q_v=1.0917E5J/mol	T_1=3418.8 K
σ_0=71.5 MPa	C=334220	Ω_0=67.1755	C_T=198.62
b=2.857E−10 m	U_0=6.9492E8m^{-1}	ρ_0=10E11 m^{-2}	α=1.0

Fig. 2 Stress–strain curves using fit parameters vs. experimental results for different strain rates at 25 °C (**a**) and 200 °C (**b**) [15]
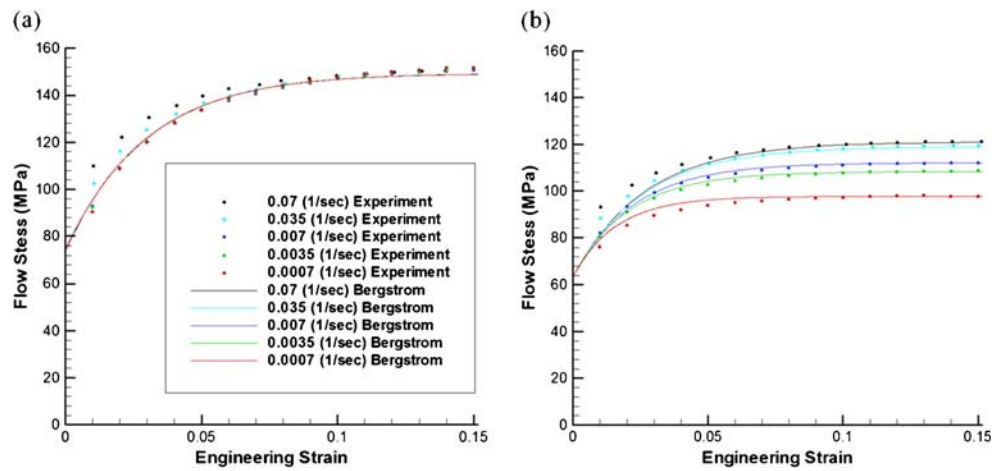
Numerical integration

The normality rule is used to obtain the plastic strain increment. From the associative flow rule:

$$\dot{\varepsilon}_{ij}^{p} = \dot{\lambda}\frac{\partial\overline{\sigma}(\sigma_{ij})}{\partial\sigma_{ij}} \tag{7}$$

The numerical procedure in updating the stress state involves finding the unknown $\dot{\lambda}$ (normality parameter). At the end of the iteration all kinematics and stresses are updated using $\dot{\lambda}$. It should be noted that $\Delta\lambda = \Delta\overline{\varepsilon}^{p}$ as follows

$$\Delta\overline{\varepsilon}^{p} = \frac{\sigma_{ij}\dot{\varepsilon}_{ij}^{p}}{\overline{\sigma}(\sigma_{ij})} = \frac{\sigma_{ij}\Delta\lambda\frac{\partial\overline{\sigma}(\sigma_{ij})}{\partial\sigma_{ij}}}{\overline{\sigma}(\sigma_{ij})} = \frac{\Delta\lambda\overline{\sigma}(\sigma_{ij})}{\overline{\sigma}(\sigma_{ij})} = \Delta\lambda \tag{8}$$

where $\Delta\overline{\varepsilon}^{p}$ is the equivalent plastic strain increment and $\overline{\sigma}(\sigma_{ij})$ is a first order homogenous function i.e. $\overline{\sigma}(\sigma_{ij}) = \overline{\sigma}(\sigma_{ij}) \times \frac{\partial\overline{\sigma}(\sigma_{ij})}{\partial\sigma_{ij}}$. To obtain $\Delta\overline{\varepsilon}^{p}$, the calculation of $\overline{\sigma}$ and $\frac{\partial\overline{\sigma}}{\partial\sigma_{k}}$ is required. The explicit forms of these terms for the Barlat YLD2000 yield function are derived by Yoon et al. [32].

The strain increments, $\Delta\varepsilon_{ij(n+1)}$, the previous total stress state, σ_{ij}, and history variables are given by the FEM code at the beginning each time step. The strain increment is assumed to be elastic first and a trial elastic stress state is calculated with the previous converged values of the state variables.

$$\sigma_{ij(n+1)}^{(trial)} = \sigma_{ij(n)} + C_{ijkl}\Delta\varepsilon_{kl(n+1)} \tag{9}$$

where C_{ijkl} is the forth order elastic tensor which is assumed to be a constant. If the new stress state lies outside the yield surface, this trial state must be corrected to calculate the elastic–plastic stress state. Using this trial stress, the yield function, $\overline{\sigma}_{(n+1)}^{(trial)}$, and its derivative, $\frac{\partial\overline{\sigma}_{(n+1)}^{(trial)}}{\partial\sigma_{ij}}$ are calculated. The size of the yield locus, $\overline{\sigma}\left(\overline{\varepsilon}_{(n+1)}^{p}, \dot{\varepsilon}, T\right)$, is calculated using the hardening rule, as presented in Eq. 1. Next it is checked whether the calculated trial stress state lies inside the yield surface using

$$\phi\left(\overline{\sigma}_{(n+1)}^{(trial)}, \varepsilon_{(n+1)}^{p}, \dot{\varepsilon}, T\right) = \overline{\sigma}\left(\sigma_{ij(n+1)}^{(trial)}\right) - \sigma\left(\overline{\varepsilon}_{(n+1)}^{p}, \dot{\varepsilon}, T\right) \leq 0 \tag{10}$$

If this condition is met, then the trial stress state is elastic and therefore is the actual stress that should be returned to FEM code. Otherwise, the material has yielded and the stress state is elastic–plastic. An iterative Newton–Raphson method is then used to return the trial stress state to the yield surface by calculating the normality factor, $\Delta\lambda$, using sub-steps m. Then, the stress state is updated for next step as

$$\begin{aligned} \sigma_{ij(n+1)}^{(m+1)} &= C_{ijkl}\left[\varepsilon_{kl(n+1)} - \varepsilon_{kl(n+1)}^{p}\right] \\ &= C_{ijkl}\left[\varepsilon_{kl(n+1)} - \varepsilon_{kl(n)}^{p}\right] - C_{ijkl}\Delta\varepsilon_{kl}^{p} \end{aligned} \tag{11}$$
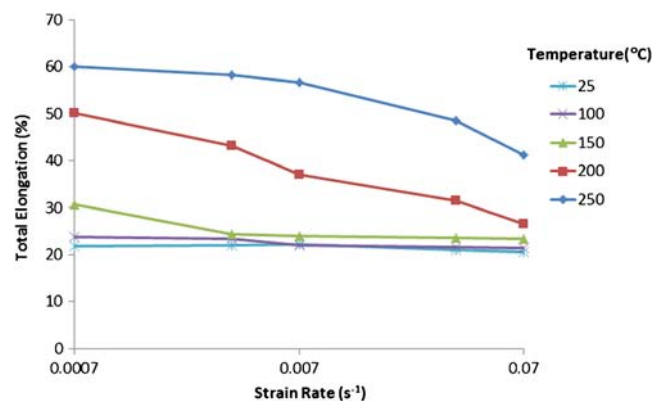

Fig. 3 Elongation to failure vs. strain rate on a logarithmic scale

Table 2 Yield stresses and R values at different temperatures for AA3003

Temperature (C)	Yield stress				R-values		
	σ_0	σ_{90}	σ_{45}	σ_b	R_0	R_{90}	R_{45}
25	78.66	71.29	75.87	77.265	0.694	0.5627	0.758
100	74.73	72.55	73.75	74.24	0.7122	0.5786	0.7642
150	69.77	69.1	70.27	70.02	0.7065	0.5807	0.7786
200	65.02	61.92	62.49	63.755	0.6981	0.6022	0.7584
250	52.8	52	51.4	52.1	0.6871	0.5906	0.7407

By combining Eqs. (7) and (11) knowing that $\sigma^{(m)}_{ij(n+1)}$ $= \sigma^{(trial)}_{ij(n+1)}$, Eq. (11) becomes

$$\sigma^{(m+1)}_{ij(n+1)} = \sigma^{(m)}_{ij(n+1)} - \Delta\lambda C_{ijkl} \frac{\partial \overline{\sigma}^{(m)}_{(n+1)}}{\partial \sigma_{ij}} \qquad (12)$$

The yield function and hardening rule are calculated using this new stress state and the yielding check is performed again.

$$\phi^{(m+1)}\left(\overline{\sigma}^{(m+1)}_{(n+1)}, \overline{\varepsilon}^{p(m+1)}_{(n+1)}, \dot{\varepsilon}, T \right)$$
$$= \overline{\sigma}\left(\sigma^{(m+1)}_{ij(n+1)} \right) - \overline{\sigma}\left(\overline{\varepsilon}^{p(m+1)}_{(n+1)}, \dot{\varepsilon}, T \right) \leq 0 \qquad (13)$$

The iteration procedure is repeated until plastic consistency is obtained to within a defined tolerance, i.e. $\phi^{(m+1)}$ $\left(\overline{\sigma}^{(m+1)}_{(n+1)}, \overline{\varepsilon}^{p(m+1)}_{(n+1)}, \dot{\varepsilon}, T \right) \leq \delta$ where δ is a small number. To solve for the normality parameter, $\Delta\lambda$, Eq. (10) is simplified using a Taylor expansion as:

$$\phi^{(m)}\left(\overline{\sigma}^{(m)}_{(n+1)}, \overline{\varepsilon}^{p(m)}_{(n+1)}, \dot{\varepsilon}, T \right) + \frac{\partial \phi^{(m)}}{\partial \sigma_{ij}}$$
$$\times \left(\sigma^{(m+1)}_{ij(n+1)} - \sigma^{(m)}_{ij(n+1)} \right) + \frac{\partial \phi^{(m)}}{\partial \overline{\varepsilon}^p}$$
$$\times \left(\overline{\varepsilon}^{p(m+1)}_{(n+1)} - \overline{\varepsilon}^{p(m)}_{(n+1)} \right)$$
$$= 0 \qquad (14)$$

From Eqs. (12) and (14) knowing that $\overline{\varepsilon}^{p(m+1)}_{(n+1)} - \overline{\varepsilon}^{p(m)}_{(n+1)} = \Delta\lambda$, the normality factor, $\Delta\lambda$, is obtained as

$$\Delta\lambda = \frac{\phi^{(m)}\left(\overline{\sigma}^{(m)}_{(n+1)}, \overline{\varepsilon}^{p(m)}_{(n+1)}, \dot{\varepsilon}, T \right)}{\frac{\partial \overline{\sigma}^{(m)}_{(n+1)}}{\partial \sigma_{ij}} C_{ijkl} \frac{\partial \overline{\sigma}^{(m)}_{(n+1)}}{\partial \sigma_{kl}} - \frac{\partial R^{(m)}_{(n+1)}}{\partial \overline{\varepsilon}^p}} \qquad (15)$$

At the end of each step, the thickness strain is calculated using a secant iteration method and is returned to the FEM code.

Fit parameters

Measured uniaxial tensile data [21] at different temperatures (25 °C, 100 °C, 150 °C, 200 °C, and 250 °C) and strain rates ($7\times10^{-4}\,\text{s}^{-1}$, $3.5\times10^{-3}\,\text{s}^{-1}$, $7\times10^{-3}\,\text{s}^{-1}$, $3.5\times10^{-2}\,\text{s}^{-1}$, and $7\times 10^{-2}\,\text{s}^{-1}$) are used to fit the Bergstrom parameters using a custom computer program written for this purpose. The fit parameters [15] are listed in Table 1. Figure 2 shows the experimental data and the curves for the Bergstrom model using the fit parameters in Table 1 at room temperature and 200 °C at different strain rates which show good agreement, particularly for strain levels beyond first yield ($\varepsilon > 3$ %). Comparison of Fig. 2(a) and (b) reveals that the material exhibits a higher strain rate sensitivity and material softening at elevated temperatures and this behaviour is captured well by the Bergstrom and Hallen [9] model.

Figure 3 shows the effects of temperature and strain rate on the total elongation to failure for the range of temperatures and strain rates considered. At room temperature, the elongation of this AA3003 aluminum alloy shows almost no rate sensitivity. At temperatures above 150 °C, the elongation is seen to

Table 3 Temperature dependent anisotropy parameters for Barlat YLD-2000 [6]

C	C	α_1	α_2	$\alpha_3 = \alpha_6$	α_4	α_5	α_7
25	0.86346	1.13930	0.94163	1.09380	1.01080	1.01010	1.10150
100	0.96053	0.99171	0.96707	1.04170	1.00990	0.99095	1.05900
150	0.98445	0.94841	0.95792	1.02420	1.00680	0.97441	1.02210
200	0.92524	1.04990	0.98358	1.05790	1.01610	1.01400	1.10640
250	0.97386	0.97141	0.99096	1.03420	1.01470	1.00050	1.08640

(a)   (b)

increase dramatically. The strain-rate sensitivity also becomes significant at higher temperature for which increases in strain rate lead to an decrease in the total elongation. The post-uniform elongation is much larger at temperatures above 200 °C than at lower temperatures. The total strain at failure is approximately 25 % at room temperature and 100 °C, while the total elongation increases by 30–50 % at 200 °C and 40–60 % at 250 °C, depending upon the strain rate. Much of this increase is attributed to the increased rate sensitivity which in turn promotes high levels of diffuse necking at high temperatures compared to room temperature conditions.

The yield stresses and the R-values in the longitudinal, transverse and diagonal directions are given in Table 2. Using these tabulated yield stresses and R-values, one can find the eight anisotropy parameters [7] at different temperatures (Table 3). For this purpose a set of eight non-linear algebraic equations are solved for α_i with a Newton–Raphson non-linear solver.

In order to capture the dependence of the yield function shape on temperature, fourth order functions are fitted to the α_i values listed in Table 3, which are given in Eq. (16).

$$\alpha_1 = 1.39 \times 10^{-9}T^4 - 7.17 \times 10^{-7}T^3 + 0.0001152T^2 - 0.005536T + 0.9405$$
$$\alpha_2 = -2.44 \times 10^{-9}T^4 + 1.27 \times 10^{-6}T^3 - 0.0002086T^2 + 0.01064T + 0.9847$$
$$\alpha_3 = -5.98 \times 10^{-10}T^4 + 3.48 \times 10^{-7}T^3 - 6.72 \times 10^{-5}T^2 + 0.004978T + 0.854$$
$$\alpha_4 = -8.34 \times 10^{-10}T^4 + 4.39 \times 10^{-7}T^3 - 7.26 \times 10^{-5}T^2 + 0.003725T + 1.04$$
$$\alpha_5 = -2.10 \times 10^{-10}T^4 + 1.16 \times 10^{-7}T^3 - 2.09 \times 10^{-5}T^2 + 0.001359T + 0.9882$$
$$\alpha_6 = \alpha_3$$
$$\alpha_7 = -9.48 \times 10^{-10}T^4 + 5.18 \times 10^{-7}T^3 - 9.15 \times 10^{-5}T^2 + 0.00564T + 0.9185$$
$$\alpha_8 = -1.99 \times 10^{-9}T^4 + 1.09 \times 10^{-6}T^3 - 0.0001931T^2 + 0.0119T + 0.9084$$

(16)

Warm forming of plate: experiment and simulation

The tooling geometry was generated based on inputs from Dana Canada which incorporated the cup feature but a

foreshortened length (Fig. 1). In normal room temperature manufacturing of the plates, multiple forming steps are required to achieve the depth of draw needed to form the cup feature within the plate geometry (Fig. 4). Note that the
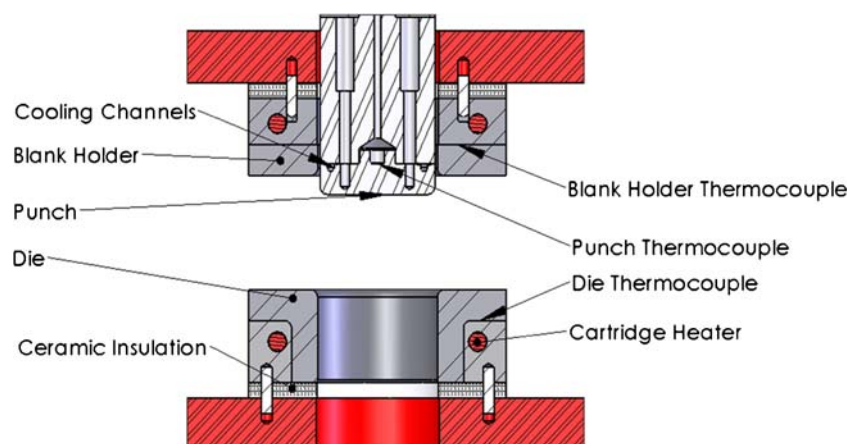
Fig. 5 Schematic view of warm tooling

Cooling Channels
Blank Holder
Punch
Die
Ceramic Insulation

Blank Holder Thermocouple
Punch Thermocouple
Die Thermocouple
Cartridge Heater

Table 4 Core plate forming process variables (for experiment and simulation)

Variable	Range
Die and blank holder temperature	Up to 300 °C
Punch temperature	15 °C
Blank holder force	2.24 kN (500 lbf) to 6.72 kN (1,500 lbf)
Bubble depth	Up to 6.8 mm
Punch speed	0.5 to 8.0 mm/s
Lubricants	Dasco Cast 1200 (μ=0.08) and Teflon sheet (μ=0.043)

hole in the deep drawn section of the cup feature is pierced after the forming step. One objective of the current work is to determine whether non-isothermal warm forming with a cold punch and heated die, would allow a plate and cup to be formed in a single draw step.

Experimental setup

Forming of the plates was performed using a specially designed warm forming toolset. A schematic view of the tooling is shown in Fig. 5, which has a heated die and blank holder as well as a cooled punch. The punch profile and die entry radii are both 2.36 mm. The die and blank holder temperatures can be set between 25 °C and 300 °C using PID controllers with thermocouple feedback loops. The punch is cooled to approximately 15 °C using a chilled water supply. The tooling can accommodate a maximum punch speed of 40 mm/s, however, punch speeds of 0.5–8.0 mm/s are used in this work. The warm forming tooling was mounted in a double-acting servo-hydraulic press. The forming process parameters are summarized Table 4. Higher levels of blank holder force were considered for the lubricant with lower coefficient of friction (Teflon sheet). The experimental setup is controlled by a Labview code which provides program signals to the servo controllers and records punch and blank holder force, punch velocity, tooling temperatures, and, optionally, the blank center temperature during forming.

Different configurations of die and punch temperatures and clamping forces are used. For all non-isothermal configurations, the punch temperature is kept cold at 15 °C while experiments were performed with the die and clamp at different temperature levels, ranging from room temperature to 300 °C.

Prior to forming, the blanks are cleaned thoroughly and either Dasco Cast 1200 lubricant is sprayed on both sides of the blank, or Teflon sheet is used as the lubricant. The forming process starts by placing the blank on the previously heated (or non-heated) die. The clamp is closed and the blank is heated by the dies and reaches the die temperature. The punch then advances to contact the blank, pushing the blank into the die cavity to a depth of 1 mm. This initial displacement is imposed to ensure that the surfaces are in contact and that heat is transferred between the die, punch and blank. The tooling is held stationary at this position for

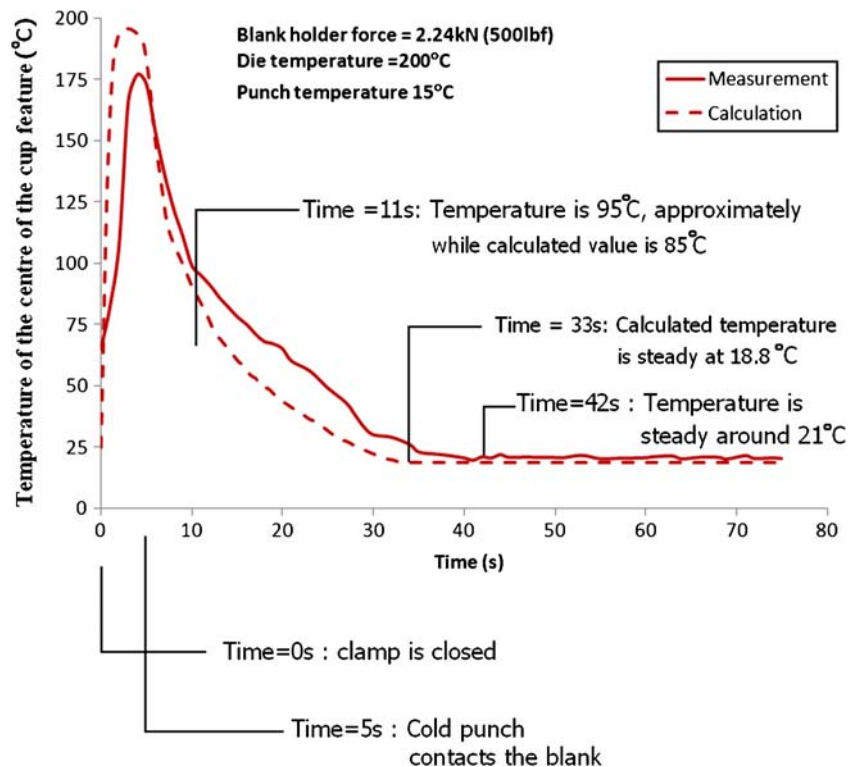**Fig. 6** Temperature of the centre of cup feature under the punch

Fig. 7 Summary of experimental results for 8 mm/s punch speed, cold punch at 15 °C for non-isothermal cases and total draw depth of 5 mm and Dasco Cast as lubricant

Clamp Force	Die Temperature		
	Room Temperature	**250°C**	**300°C**
2.24kN	Failure, severe wrinkling	Failure, severe wrinkling	No failure, moderate wrinkling
4.48kN	Failure, moderate wrinkling	Failure, mild wrinkling	Failure (necking), no wrinkling

30 s while the region of the cup under the punch is cooled by the punch. Finally, the punch movement is activated to force the blank into the die cavity, forming the cup shaped part, with or without failure. Figure 6 shows the recorded and predicted temperature history at the center of the plate cup under the punch prior to forming, for the case of 200 °C dies, a 15 °C punch and a clamping force of 2.24 kN. The calculated heating and cooling rate is faster than the measured rate of change, however both reach a steady state close to room temperature. This difference in heating and cooling rate is attributed to the Teflon lubricant which is expected to have a lower heat transfer coefficient than conventional forming lubricants. Future work will consider characterization of the heat transfer coefficient between the workpiece and tooling for a range of lubricants.

The measurement shows that the temperature of the centre of the plate cup feature is steady around 21 °C after 42 s while the model predicted a steady state at 18.8 °C after

33 s. It proved difficult to acquire transient temperature data during the actual forming operation since the thermocouple detached from the sheet surface, however, measurements such as those in Fig. 5 were used to confirm the thermal conditions prior to forming and to determine the required wait time prior to activating the punch forming motion.

Experimental results

To study the effect of temperature gradient on formability of the part, experiments considering three levels of die temperature, two levels of clamping force and two levels of punch speed have been performed. Each configuration was tested
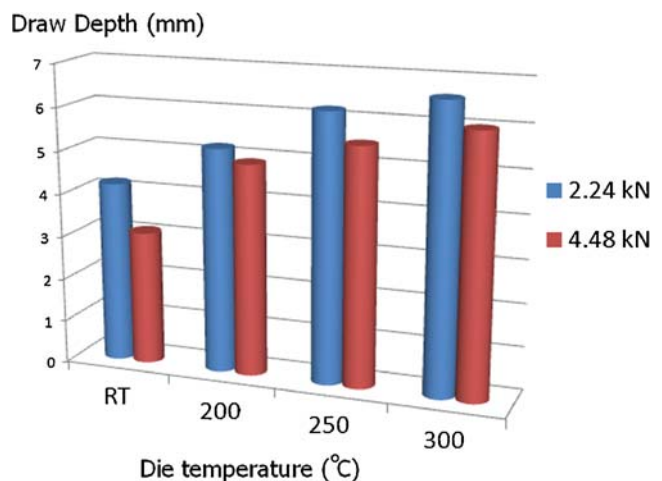
Table 5 Maximum draw depth without failure or necking at different temperature settings, using a blank holder force of 4.48 kN and punch speed of 8 mm/s

Die temperature (°C)	Punch temperature (°C)	Bubble depth (mm)	
		Dasco Cast	No lubricant
25	25	2.8	2.8
150	15	3.0	2.9
200	15	4.7	3.9
250	15	5.2	4.3
300	15	6.0	5.0

Fig. 8 Maximum draw depth before fracture (punch speed of 8 mm/s, cold punch at 15°C and Dasco Cast lubricant)

Fig. 9 Summary of experimental results for 8 mm/s punch speed, 4.48 kN clamping force, cold punch at 15°C for non-isothermal cases and total draw depth of 6.8 mm and Teflon sheet as lubricant

Room Temperature	250°C	300°C
Failure	Draw (severe wrinkling)	Draw (mild wrinkling)

at least three times to ensure repeatability. No significant difference was observed in the results for two levels of punch speed which implies that strain rate sensitivity was not significant at the velocity range of the current experiments (0.5 to 8 mm/s).

Dasco Cast lubricant experiments

Figure 7 shows the specimen condition after a total draw depth of 5 mm for room temperature isothermal and non-isothermal forming with a punch speed of 8 mm/s using Dasco Cast lubricant. For all cases, the temperature of the centre of blank under the punch was measured to be approximately 20 °C prior to forming. The forming outcomes in the figure correspond to the indicated blank holder force and die temperatures. It is evident from Fig. 7 that applying a higher clamping force reduces the degree of wrinkling; however, the elevated clamping force may result in necking or failure (tearing). The use of the elevated temperatures causes the wrinkles to reduce dramatically. The room temperature samples failed for all configurations of clamping force and punch velocity; however, for the higher punch velocity and higher clamping force, the failure initiates at a lower drawing depth. Heating the dies to 300 °C causes necking to disappear, but some wrinkles remain for a clamping force of 2.24 kN. When the clamping force is increased to 4.48 kN, necking is observed at the die entry radius of the part.

For a given blank holder force of 4.48 kN the forming was performed at different temperature configurations with and without the lubricant applied. The maximum draw depths before necking have been measured at the point of initiation of a sharp drop in punch force. A summary of these results is shown in Table 5.

The conditions summarized in Table 5 have been repeated with a punch speed of 4 mm/s; however no significant change in the results was observed. The beneficial effect of temperature difference between the cup center under the punch and the die entry radius is evident from the results. Also, it can be seen that the lubricant (Dasco Cast) has an important effect on formability at higher temperature. For temperatures lower than 150 °C, Dasco Cast does not function well as a lubricant.

Figure 8 compares the maximum draw depth (without necking) for 2.24 kN and 4.48 kN blank holder force with a punch speed of 8 mm/s under room temperature and non-isothermal forming conditions with heated dies and a cold punch at 15 °C. As seen in the figure, the draw depth increases as the blank holder force decreases. The maximum possible draw depth without necking at room temperature was observed to be 4.2 mm for a clamping force of 2.24 kN (500 lbf); however, there is significant wrinkling around the drawn cup. For dies heated at 200 °C, the part fails at a draw depth of 4.9 mm with a clamping force of 4.48 kN (1,000 lbf). By applying a clamping force of 2.24 kN, the

Fig. 10 Forming using Teflon sheet as lubricant, 6.72 kN clamping force, heated dies at 300°C and cold punch at 15°C
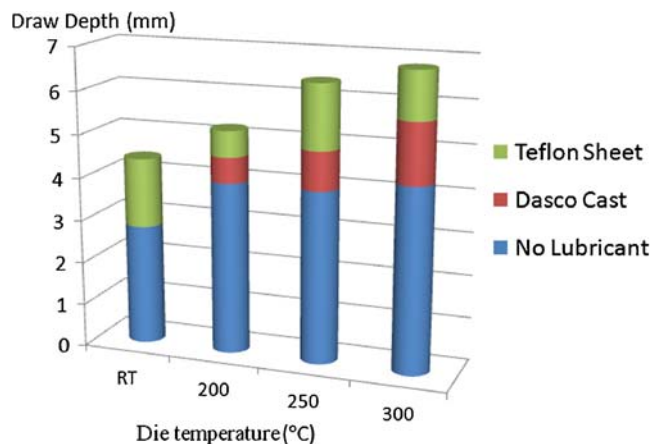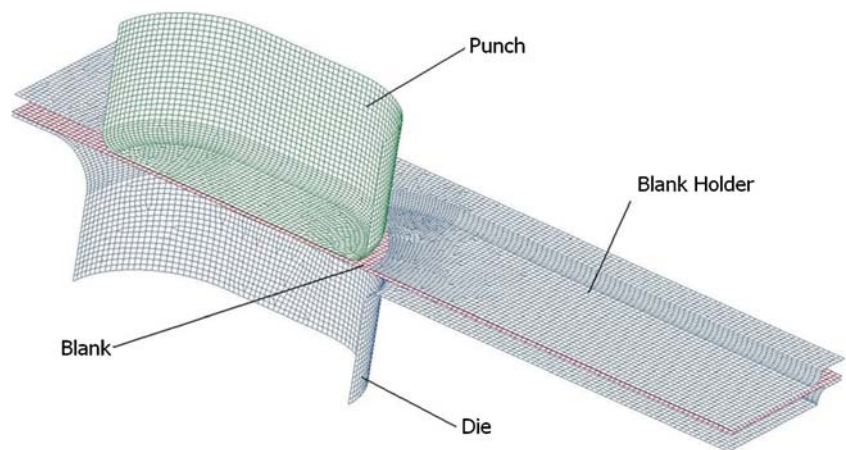

Fig. 11 Forming improvement by using Teflon sheet at different die temperatures; cold punch at 15°C, clamping force of 4.48 kN and punch speed of 8 mm/s

Fig. 12 Mesh model of tooling and blank

part can be drawn without necking (Fig. 7), however moderate wrinkling is observed.

Teflon sheet lubricant experiments

Experiments were also performed using Teflon sheet as a lubricant to overcome some of the undesirable effects of the Dasco Cast lubricant (elevated friction coefficient and build-up of residual lubricant). These experiments utilized a clamping force of 4.48 and 6.72 kN and three die temperature cases were considered: room temperature, 250 °C and 300 °C. All parts were drawn to full depth (6.8 mm). Figure 9 shows the formed parts. It can be seen that the use of Teflon sheet has improved the forming process. The forming at room temperature resulted in a broken part. Heating the dies up to either 250 or 300 °C resulted in formed part without failure though wrinkles still exist in both cases. The formed part at 300 °C showed a smaller degree of wrinkling.

To eliminate the wrinkles, the clamping force was increased to 6.72 kN (1,500 lbf) using a die temperature of 300 °C. The wrinkles disappeared although a small amount of necking was observed at the punch radius (Fig. 10). It should be noted that the parts all show a feature that appears in the photograph to be a neck at the die entry radius. This is in fact not a neck, but a lighting artifact that proved difficult to eliminate.

Figure 11 summarizes the overall forming performance for samples without lubricant and with either Dasco Cast or Teflon lubrication at different temperatures. The draw depths for forming under different temperature settings, a punch speed of 8 mm/s and a clamping force of 4.48 kN using Teflon sheet were measured and compared with those of no-lubricant forming (Table 5). The red-coloured portions indicate the improvement in formability using Dasco Cast and the green-coloured portions are the further improvement achieved using Teflon sheet, which is seen to be significant. As can be seen, the Dasco Cast has no effect at room temperature, however, it improves the draw depth by 11.3 %, 17 % and 13.2 % under non-isothermal forming conditions with dies heated to 200 °C, 250 °C and 300 °C, respectively. The ineffectiveness of Dasco Cast at room temperature was expected since it is designed for high temperature applications. The Dasco Cast has to be sprayed on the hot surface of the tooling to establish a low-friction layer in contact with the hot tool. The Teflon sheet caused a significant increase in maximum draw depth at room temperature (42 % more with respect to no-lubricant forming). The draw depths were increased by 18.1 %, 36.1 % and 28.3 % under non-isothermal forming conditions with heated at 200 °C, 250 °C and 300 °C, respectively. It was observed that the highest improvement of both

Fig. 13 Temperature distribution in a formed part with tooling at 200 °C and cold punch at 15 °C; **a** 1 mm punch depth, **b** 3 mm punch depth, and **c** 6 mm punch depth
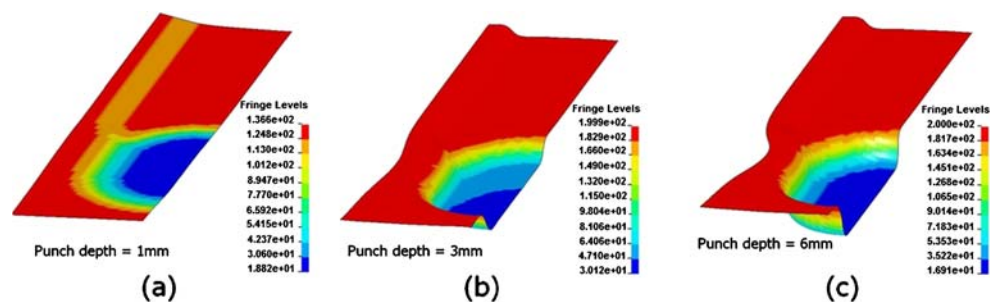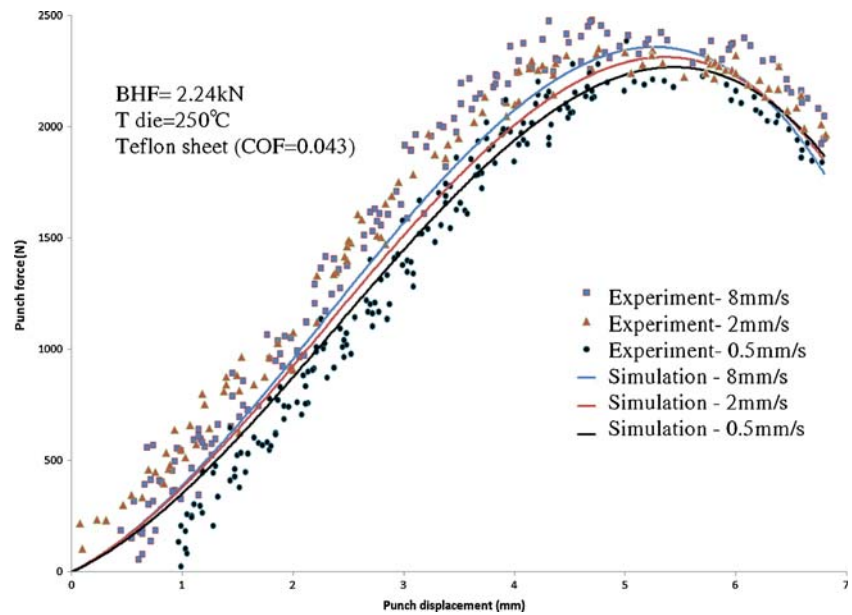
Fig. 14 Punch force vs. punch displacement for different forming speeds. Experimental results are shown with *symbols* and numerical results are in *solid lines*

lubricants (Dasco Cast and Teflon Sheet) was realized at 250 °C; however, it was necessary to heat the tooling up to 300 °C (using Teflon sheet) to draw the full depth without necking.

Numerical simulation

The solid model CAD surface descriptions of the tooling were developed as part of this work using SolidWorks. The geometry model was imported into Hypermesh and was simplified to retain just the necessary surfaces for meshing of the tooling surfaces within the finite element model. An LS-DYNA-compatible mesh was generated in Hypermesh,

as shown in Fig. 12. Due to symmetry, only one-half of the part and tooling is modeled. The mesh was generated using 4-node Belytschko-Tsay shell elements [8]. The tooling was modeled using rigid surface elements. An overall element size of 0.5 mm was used for mesh generation, but a finer mesh was used in areas near curved tooling profile radii. In total, 4,672 shell elements and 14,764 rigid elements were used for the blank and tooling, respectively.

All surface contacts are modeled as thermal contacts within LS-DYNA to simulate the heat transfer between the hot dies, cold punch and blank. The heat transfer conductivity of the contact surfaces with closed gaps is defined to be $50,000\,W/m^2K$ [11]. Intermittent mechanical contact is

Fig. 15 Comparison of punch load vs. punch displacement for different die temperatures. Experimental results are shown with *symbols* and numerical results are in *solid lines*
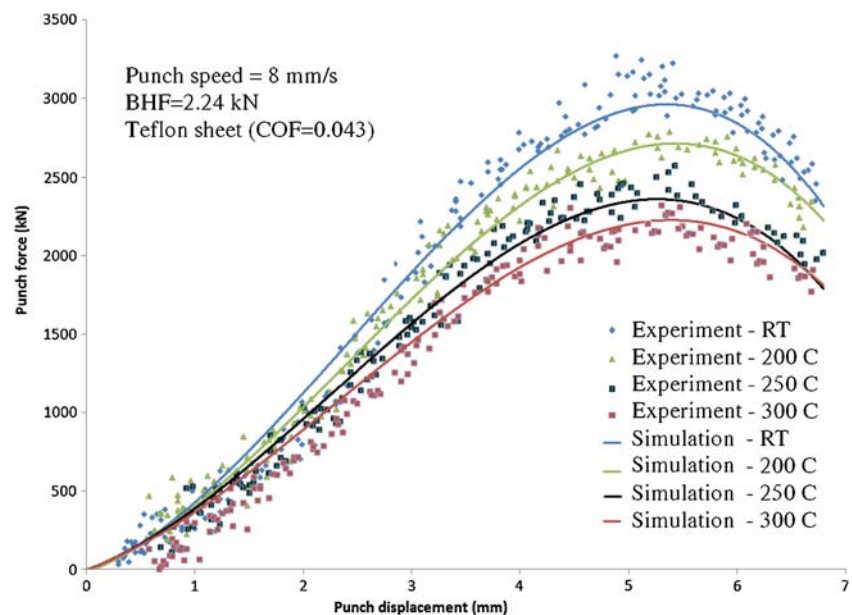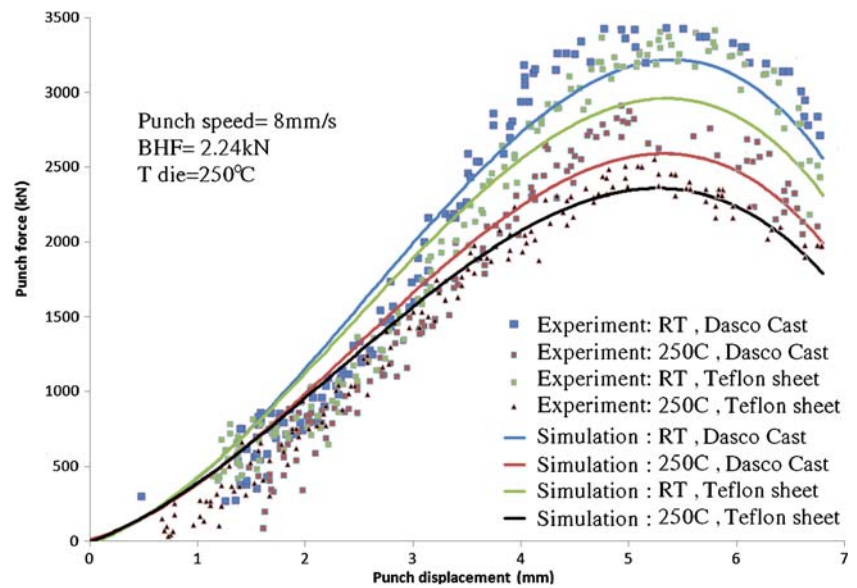
Fig. 16 Comparison of punch load for Teflon sheet and Dasco Cast as lubricants. Experimental results are shown with *symbols* and numerical results are in *solid lines*

also enforced between the blank and tooling components utilizing a penalty function-based approach. The room temperature coefficient of friction, obtained using twist compression testing for the applied lubricants and sheet material, was measured as 0.08 for Dasco Cast and 0.043 for Teflon sheet at all contact surfaces.

The loading mimics that in the experiments. The clamp die is closed first and the punch advances to push the blank into the die cavity to a depth of 1 mm. There is a pause, as described in "Experimental results" section, for heat transfer to occur after which the punch moves to desired depth. An accelerated loading rate is used in the forming experiments to keep the explicit dynamic run times manageable. The punch speed is increased by a factor of 1,000. As a result, the heat conductance coefficients between the contact surfaces and

within the blank are increased proportionally. This approach greatly reduced the required CPU time without introducing excessive dynamic effects in the simulations; the calculated kinetic energy was negligible comparing to the calculated total energy. Numerical simulations corresponding to all of the experiments have been performed. The forming process parameters used in each of the experiments have been simulated in a coupled thermo-mechanical model.

Numerical results

Temperature distribution

Accurate modelling of the temperature distribution within the sample during the warm forming procedure is important.

Fig. 17 Effect of blank holder force on punch force. Experimental results are shown with *symbols* and numerical results are in *solid lines*
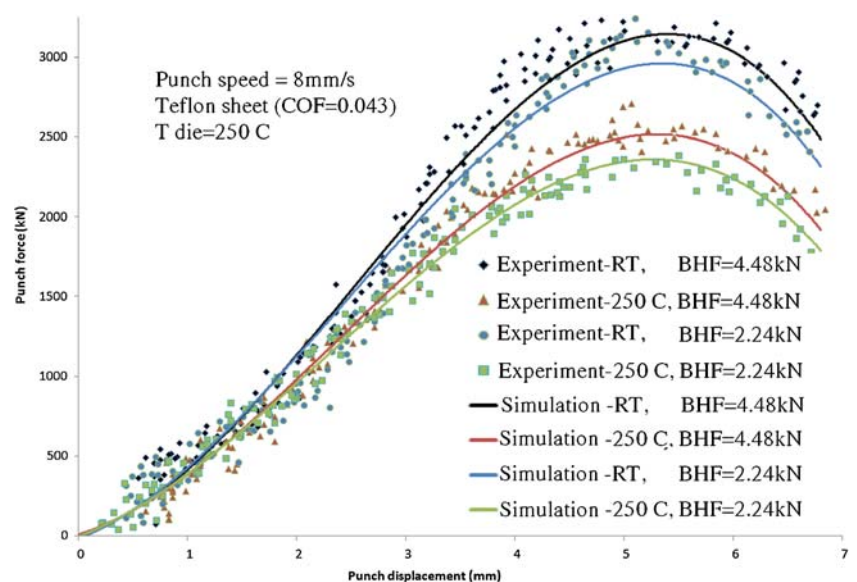
Fig. 18 Thickness reduction percentage under isothermal forming condition at **a** room temperature and **b** 300 °C and non-isothermal forming condition with warm dies at **c** 250 °C and **d** 300 °C

(a) Isothermal at room temperature (b) Isothermal at 300°C (c) Non-isothermal with dies at 250°C (d) Non-isothermal with dies at 300°C
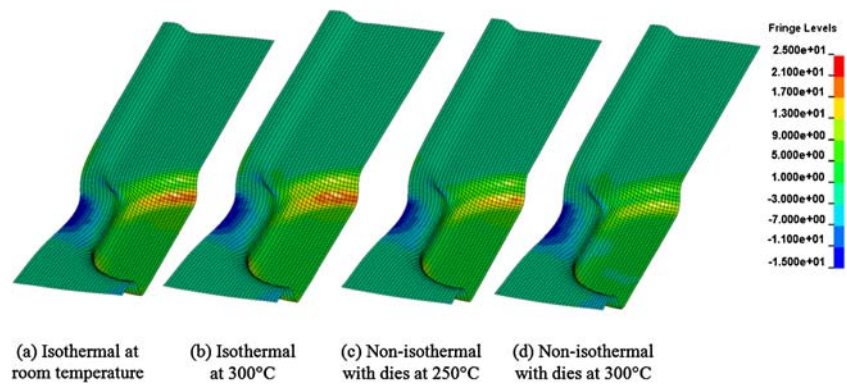
Figure 13 shows contour plots of temperature distribution at start of draw, mid-draw and end of the forming for the case in which the die and blank holder temperature is 200 °C, a clamping force of 2.24 kN is applied and the punch speed is 8 mm/s. The simulation shows that after closing the clamp and initial contact of the punch (punch depth of 1 mm), the temperature of the blank area in contact with the punch drops to approximately 19 °C while the temperature of the rest of the blank reaches the die temperature at 200 °C, very quickly. The predicted temperature time history is plotted in Fig. 5 and compares reasonably well with the measured data. Once the forming proceeds, the temperature of the blank under the punch increases to approximately 30 °C at the middle of forming step (punch depth of 3 mm), likely due to loss of contact with the punch bottom once forming starts. By the end of forming, the punch cools down the region of blank adjacent to the punch surface to 16 °C while the area between the die and binder is heated to 200 °C.

Predicted punch force

Figure 14 shows the effect of forming speed on punch force and serves to compare the experimental and numerical results. A clamping force of 2.24 kN with heated dies at 250 °C and Teflon sheet (μ=0.043) as lubricant is used. In general, the agreement between the predicted and measured punch force is good. The measured punch force data is unfiltered and exhibits a fair level of scatter. This "noise" is attribute to the rather low punch force range needed to form the cup feature (3,500 N) compared to the press capacity (896,000 N). Both experiments and simulations show that the forming speed with the studied range does not have a significant effect on punch force. Hence, for the rest of the simulations only a punch speed of 8 mm/s is considered.

Figures 15, 16 and 17 show the effect of temperature, lubricant and blank holder force on forming force comparing both experimental and numerical data. Figure 15 shows the punch force variation for different die temperature settings. For all cases, the punch speed and blank holder force are set to 8 mm/s and 2.24 kN, respectively, and Teflon sheet

lubricant is used. The increase in temperature results in a decrease in punch force. A 300 °C die temperature lowers the punch force by 29 % with respect to that of room temperature forming. Figure 16 is a comparison of punch force versus punch displacement for two different lubricants. In the simulations and experiments, the punch speed of 8 mm/s and a clamping force of 2.24 kN is used while the dies are heated to 250 °C and the punch is kept cold at 15 °C. Both cases follow the same trend with the lower friction resulting in lower punch force as expected. The effect of clamping force on punch force is shown in Fig. 17. Two blank holder forces of 2.24 kN and 4.48 kN are compared. The figure shows a very good agreement between the experimental and numerical results. Forming with higher blank holding pressure requires a higher punch force.

Effect of temperature difference between the dies and the punch on as-formed thickness

The simulations show that a higher temperature gradient at the cup wall results in less thickness reduction. Figure 18 allows comparison of the percentage thickness reduction at a draw depth of 5 mm for a clamping force of 2.24 kN and punch speed of 8 mm/s for isothermal forming conditions at (a) room temperature and (b) 300 °C; and, non-isothermal forming with a cold punch at 15 °C and dies at (c) 250 °C and (d) 300°. A coefficient of friction equal to 0.08 is used in the simulations corresponding to the Dasco Cast lubricant. It can be seen that the maximum thinning occurs at the punch profile radius. The parts formed isothermally at room temperature and at 300 °C both exhibited sharp thickness reductions. The contours also show that the non-isothermal parts experience less thickness reduction and that higher temperature gradient favours lower thickness reduction. The effect of the temperature difference between the dies and the punch on formability of the part is clearly beneficial which is in agreement with the experimental observations (Figs. 7 and 9).

Figure 19 shows the predicted and measured thickness reduction as a function of die temperature. The data
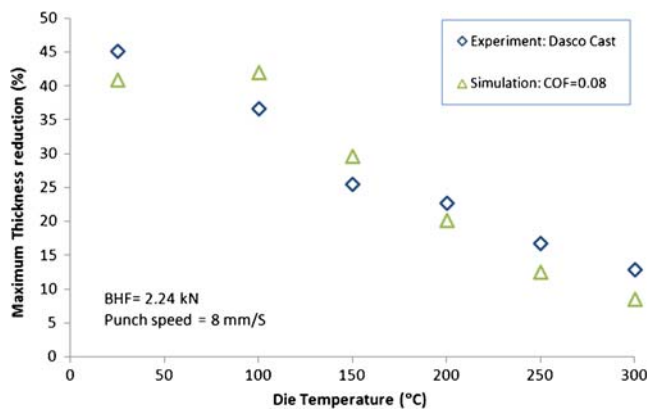
Fig. 19 Maximum thickness reduction percentage for different die temperatures

corresponds to a clamping force of 2.24 kN and punch speed of 8 mm/s. A coefficient of friction equal to 0.08 is used in the simulations corresponding to the Dasco cast lubricant. In general, the predictions agree well with the measurements.

One simplified design criterion often used in industrial practice is to specify a limit on the maximum thickness reduction, following the approach of Kim et al. [17]. In the current work, for example, if a maximum thickness reduction of 20 % was specified, the data in Fig. 18 indicates that a die temperature warmer than 200 °C would be required for successful forming.

Effect of forming parameters on thickness reduction predictions

Figure 20 shows the effect of different forming parameters on the predicted maximum thickness reduction for non-isothermal forming with dies at 250 °C and a 15 °C punch. All predictions are shown for a punch depth of 5.0 mm. Simulations were also performed for isothermal forming at room temperature and 250 °C; however, all of the isothermal models localized (failed) which indicates the importance of the non-isothermal process.

Figure 20a show the effect of punch speed on thickness prediction. All simulations were performed with a blank holder force of 2.24 kN and a coefficient of friction of 0.08. As seen, the forming speed has only a mild effect on thickness reduction, the most significant change occurring for the increase in punch speed from 0.5 to 2.0 mm/s. The maximum thickness reduction percentage was predicted as 12.5, 11.9, and 9.7 % for punch speeds of 8, 2, and 0.5 mm/s, respectively.

Figure 20b shows the predictions of maximum thickness reduction for parts formed with a punch seed of 8 mm/s and coefficient of friction of 0.08. As can be seen, the blank holder has an important effect on necking in the blank. The predicted maximum thickness reduction
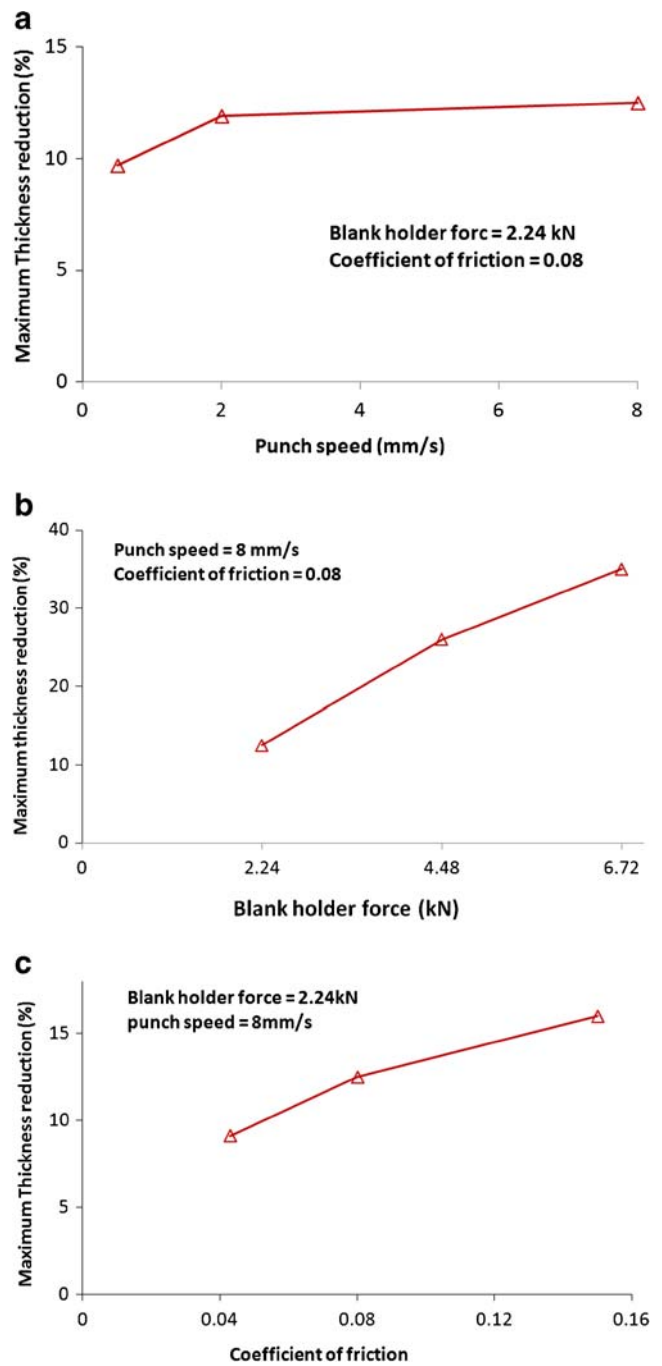

Fig. 20 Effect of forming parameters on predicted maximum thickness reduction percentage for non-isothermal forming with warm dies at 250 °C and cold punch at 15 °C: **a** effect of punch speed, **b** effect of blank holder force, and **c** effect of friction

increased almost linearly with increases in the blank holder force. The predicted maximum thickness reduction using a blank holder force of 2.24 kN was 12.5 % for non-isothermal forming with dies at 250 °C. Increasing the blank holder force from 2.24 kN to 4.48 kN and to 6.72 kN resulted in increases in thickness reductions of 26 % and 35 %, respectively.

Friction was also identified as an important factor in controlling localized necking. Figure 20c shows the predicted maximum thickness reduction using a punch speed of 8 mm/s, blank holder force of 2.24 kN, and three different coefficients of friction; i.e. 0.15, 0.08, and 0.043. The thickness reduction increased with increases in friction; the predicted values of thickness reduction were 9.1 %, 12.5 %, and 16 % for coefficients of friction of 0.15, 0.08, and 0.043, respectively.

Discussion and conclusion

Experiments on warm forming of a cup shaped feature within the modified AA3003 plates have shown that application of independent die and punch temperature control increases the formability of AA3003 aluminum alloy sheet. Increasing the difference in temperature between the punch and the die improves the formability. This result is consistent with studies of a number of 5000-series alloys by Takuda et al. [29], Palumbo and Tricarico [25] and Kaya et al. [16]. By considering a maximum thickness reduction of 20 % as a simplified design criterion, a minimum die temperature of 200 °C is required to draw the part. Warm forming has an important effect on the thickness within the part sidewall and reduces thinning at the punch radius. Also, friction has an important effect on thinning, while forming speed has a negligible effect on the punch force for the range considered in this work. Numerical models incorporating the Bergstrom hardening model [9] and Barlat's Yld2000 yield surface [6] were found to accurately predict the mechanical behaviour of AA3003. The simulations are capable of capturing both punch force and failure location for the studied material. The parametric study showed that forming speed does not have a significant effect on localized necking for the range of punch velocities in this study. On the other hand, both friction and blank holder force are identified as important forming parameters in controlling the thickness reduction in the blank.

The current paper focuses on the benefits associated with non-isothermal forming in cup drawability, using simplified failure criteria, such as thickness reduction limits, for example. The major benefit associated with non-isothermal forming is attributed to the mechanical increase in strength at the punch nose (low temperature region) and increase in ductility at the flange region (elevated temperature region). The effect of temperature on the forming limit of this AA3003 alloy (in the absence of temperature gradient) is also under investigation. Bagheriasl [3] has demonstrated that formability increases dramatically in elevated temperature LDH testing of this alloy. The incorporation of forming limit criteria within finite element simulation of warm forming operations is the topic of on-going research.

References

1. Abedrabbo N, Pourboghrat F, Carsley J (2006) Forming of aluminum alloys at elevated temperatures—part 1: material characterization. Int J Plast 22(2):314–341
2. Abedrabbo N, Pourboghrat F, Carsley J (2007) Forming of AA5182-O and AA5754-O at elevated temperatures using coupled thermomechanical finite element models. Int J Plast 23(5):841–875
3. Bagheriasl R (2012) Formability of aluminum alloy sheet at elevated temperature. PhD thesis, University of Waterloo
4. Bagheriasl R, Ghavam K, Worswick MJ (2011a) Formability analysis of aluminum alloy sheets at elevated temperatures with numerical simulation based on the M-K method, Proc. of ESAFORM, Belfast, Ireland
5. Bagheriasl R, Ghavam K, Worswick MJ (2011) Effect of strain rate and temperature gradient on warm formability of Aluminum alloy sheet. NUMISHEET, Seoul
6. Barlat F, Brem JC, Yoon JW, Chung K, Dick RE (2003) Plane stress yield function for aluminum alloy sheets—part 1: theory. Int J Plast 19:1297–1319
7. Barlat F, Yoon JW, Cazacu O (2007) On linear transformations of stress tensors for the description of plastic anisotropy. Int J Plast 23 (6):876–896
8. Belytschko T, Tsay CS (1981) Explicit algorithms for nonlinear dynamics of shells. AMD ASME 48:209–231
9. Bergstrom Y, Hallen H (1982) An improved dislocation model for the stress–strain behavior of polycrystalline α-Fe. Mater Sci Eng 55:49–61
10. Boogaard AH, Huetink J (2006) Simulation of aluminum sheet forming at elevated temperatures. Comput Methods Appl Mech Eng 195:6691–6709
11. Cengel YA, Boles MA (2001) Thermodynamics: an engineering approach, 4th edn. McGraw-Hill
12. Farrokh B, Khan AS (2009) Grain size, strain rate, and temperature dependence of flow stress in ultra-fine grained and nanocrystalline Cu and Al: synthesis, experiment, and constitutive modeling. Int J Plast 25:715–732
13. Ghavam K, Naghdabadi R (2011) Constitutive modeling of temperature and strain rate dependent elastoplastic hardening materials using a corotational rate associated with the plastic deformation. Int J Plast 27:1445–1455
14. Ghavam K, Bagheriasl R, Worswick MJ (2011a) Numerical modeling of hemispherical dome testing of aluminum alloy sheet at elevated temperatures, Int. Symp. of Plasticity, Puerto Vallarta, Mexico
15. Ghavam K, Bagheriasl R, Worswick MJ (2011b) Stress analysis of non-isothermal deep drawing with induced anisotropy and rate sensitivity at elevated temperatures, Submitted to JMPT
16. Kaya S, Spampinato G, Altan T (2008) An Experimental Study on Nonisothermal Deep Drawing
17. Kim HS, Koc M, Ni J, Ghosh A (2006) Finite element modeling and analysis of warm forming of aluminum alloys-validation through comparisons with experiments and determination of a failure criterion. J Manuf Sci Eng Trans ASME 128:613–621
18. Kurukuri S, Boogaard AH, Mirox A, Holmedal B (2009) Warm forming simulation of Al–Mg sheet. J Mater Process Technol 209 (15–16):5636–5645

19. Kurukuri S, Miroux A, Wisselink HH, Boogaard AH (2011) Simulation of stretch forming with intermediate heat treatments of aircraft skins—a physically based modeling approach. Int J Mater Form 4(2):129–140

20. Li D, Ghosh A (2003) Tensile deformation behavior of aluminum alloys at warm forming temperatures. Mater Sci Eng A Struct 352:279–286

21. Mckinley J (2010) Warm forming of aluminum brazing sheet. MSc thesis, University of Waterloo

22. Mckinley J, Abedrabbo N, Worswick MJ, Kozdras M (2008) Effect of independent die and punch temperature control on the formability of 3003 aluminum alloy in warm deep drawing. Proc. of the 7th Int. Conf. Numisheet, Interlaken, Switzerland

23. Naka T, Yoshida F (1999) Deep drawability of type 5083 aluminum–magnesium alloy sheet under various conditions of temperature and forming speed. J Mater Process Technol 89/90:19–23

24. Nes E (1998) Modeling of work hardening and stress saturation in FCC metals. Prog Mater Sci 145:129–193

25. Palumbo G, Tricarico L (2007) Numerical and experimental investigations on the warm deep drawing process of circular aluminum alloy specimens. J Mater Process Technol 184:115–123

26. Schmoeckel D (1994) Temperaturgefü̈hrte Prozeßsteuerung beim Umformen von Aluminiumblechen. EFB-Forschungsbericht Nr. 55

27. Schmoeckel D, Liebler BC, Speck FD (1995) Grundlagen und modellversuche-temperaturgeführterstofffluß beim tiefziehen von Al-blech-realversuche. Bander Bleche Rohre 36:14–21

28. Shehata F, Painter MJ, Pearce R (1978) Warm forming of aluminum/magnesium alloy sheet. J Mech Work Technol 2:279–291

29. Takuda H, Mori K, Masuda I, Abe Y, Matsuo M (2002) Finite element simulation of warm deep drawing of aluminum alloy sheet when accounting for heat conduction. J Mater Proc Technol 120:412–418

30. Tebbe PA, Kridli GT (2004) Warm forming of aluminum alloys: an overview and future directions. Int J Mater Prod Technol 21:24–40

31. Wilson DV (1988) Aluminum versus steel in the family car—the formability factor. J Mech Work Technol 16:257–277

32. Yoon J, Barlat F, Dick RE, Chung K, Kang TJ (2004) Plane stress yield function for aluminum alloy sheets-part II: FE formulation and its implementation. Int J Plast 20(3):495–522